Smart Rocks and Wireless Communication Systems for Real-Time Monitoring and Mitigation of Bridge Scour
(Progress Report No. 3)

Contract No: RITARS-11-H-MST
(Missouri University of Science and Technology)

Ending Period: March 31, 2012

PI: Genda Chen
Co-PIs: David Pommerenke and Rosa Y. Zheng

Program Manager: Mr. Caesar Singh

Submission Date: April 19, 2012

TABLE OF CONTENTS

EXECUTIVE SUMMARY

In the third quarter, the following main components were addressed: 1) effects of outside volume of permanent magnets (passive smart rocks) on signal strength, 2) “frictionless” smart rocks with embedded magnets wrapped with electric coil as active sensors, 3) final design and test of a magneto-inductive communication system with small smart rocks (active smart rocks), and 4) acoustic communication protocol, implementation, and evaluation.

With the same outside dimension, a hollow sphere and a solid sphere have the same signal strength. As such, the hollow sphere is more effective than the solid sphere. A prototype of embedded magnet smart rock that is controllable with a coil has been designed and built; it will be tested for its superior sensitivity.

Prototypes of magneto-inductive smart rocks were further refined and improved for more complete functionality. They will be ready for laboratory tests. Necessary software continues to be developed and will be used in laboratory tests.

I - TECHNICAL STATUS

I.1 ACCOMPLISHMENTS BY MILESTONE

Task 1.1 Optimal Passive Smart Rock – Engineering Design and Validation of DC Magnetic Passive Smart Rocks

Specific Objectives

In the past quarter, measurements of a smart rock are characterized for the following purposes: 1) continued quantification of the effects of various sized and shaped magnets, 2) angle optimization of the magnet with relation to Earth's magnetic gradient, 3) development and testing of waterproof encasements for early prototypes of both active and passive smart rocks.

Preliminary Results on Magnetic Effects: In the following discussion, magnetic fields of permanent magnets in various shapes are measured and discussed including solid and hollow cylindrical shaped magnets (inside diameter of ¼"). The magnets tested and reported in this quarterly report used the same magnet materials with high grade Neodymium, Grade N45 (12,500 gauss) by the United Nuclear Scientific LLC. All tests were performed in the same empty football field for test consistency and minimization of the disturbance of potential metal objects near the test site. In addition, angle optimization was accomplished by using a bi-axial rotation apparatus that was custom designed for this project and will be discussed further in this report.

Strength Gradient-Distance Curves: In an attempt to find a lighter magnet to reduce weight in the passive smart rock prototype, the intensity of the magnetic field and vertical gradient of a solid magnetic rod, with diameter of ½ in. and length of 1 in., were tested and compared to that of a hollow tube magnet, with the same length and outer diameter but an interior diameter of ¼". The test procedures are similar to tests performed for various magnet shapes described in previous quarterly reports. To test the intensity of the magnetic field of each magnet, the magnetometer G-858 was held in a stationary position while each magnet moved at a constant speed in a straight line up to a distance of 40 ft away from the sensor. Likewise, to find the gradient, each magnet moved along this same path while rotating at a constant speed every foot up to 40 ft.

Figure 1 (a) shows a comparison of the average field intensities of two tested magnets. Similarly, Figure 1 (b) compares their vertical gradient. With the same length and outer diameter, the material reduction of the magnet does not affect much to the intensity nor the gradient of the magnetic field. Therefore, using hollow magnets instead of solid magnets will provide similar sensing strength with less magnet weight and lower cost, indicating that the magnetic field strength of the smart rock could be potentially increased to a large extent by enclosing the smart rock in a large hollow steel bowl or as such.

Angle Optimization: To determine the best angle for a ½" x 1" cylindrical rod magnet a constant rotation apparatus was developed to allow for simultaneous rotation about two axes as shown in Figure 2 for the test setup. Three different tests were performed: horizontal axis rotation, vertical axis rotation, and finally biaxial rotation. The Magnetometer G-858 was stationed 5 feet away from the rotating apparatus during all of these tests, and multiple runs were performed.

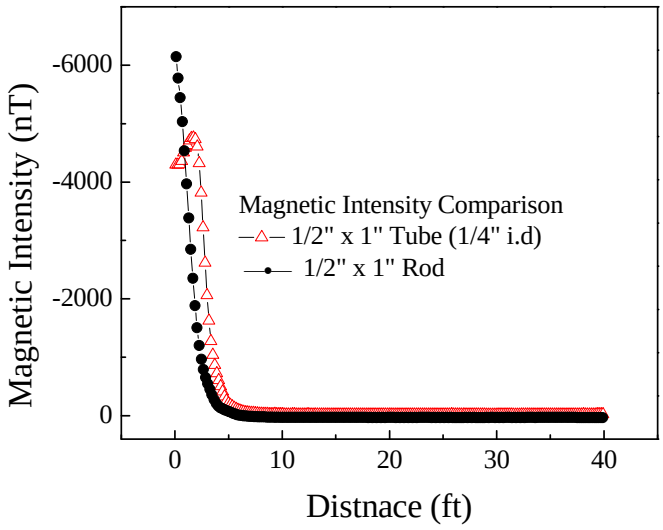

(a) Comparison of magnetic field intensity

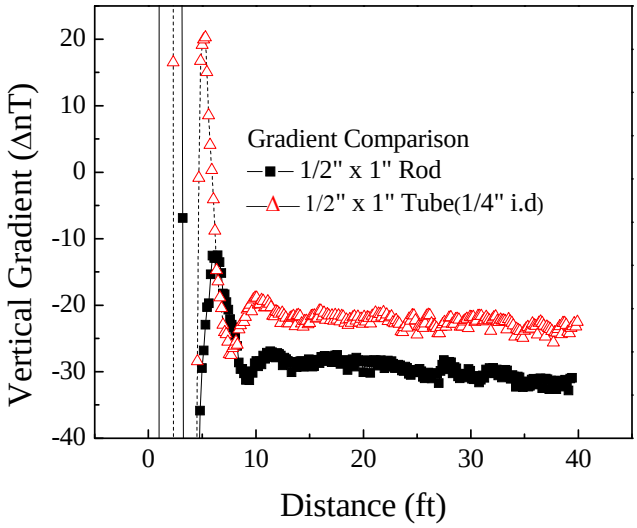

(b) Comparison of vertical gradient

Figure 1: ½" x 1" solid cylindrical magnet vs. ½" x 1" hollow cylindrical magnet (1/4" i.d.)

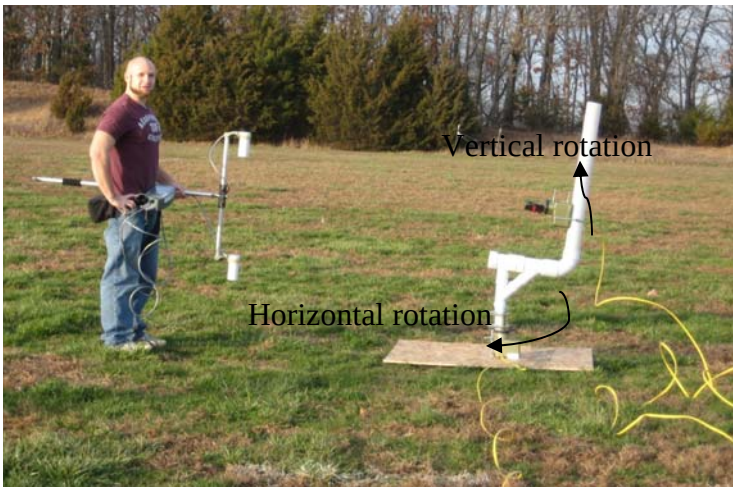

Figure 2: Bi-axial rotation apparatus

Tests involved rotations in horizontal, vertical plan, and bi-axial plane. The test results were averaged and plotted as shown in Figures 3 (a-c), respectively. Figures 3 (a, b) show that in both horizontal and vertical plane, the intensity of the magnetic field yields maximum when the magnet rotated to a location when the magnet is normal to the sensor and minimum when the magnet is parallel to the sensor. Figure 3 (c) indicates that the maximum vertical gradient reading occurs around 19 and 44 seconds, respectively. With this particular time period and a constant rotation speed of one revolution per minute, the angles when the maximum intensity of magnetic field can be determined and estimated as following:

$$\frac{19}{60}\times 360 = 114, \qquad \frac{44}{60}\times 360 = 250$$

Therefore, the rod magnets were estimated to obtain their maximum vertical gradient reading when the angle of the rod is 114 ° and 250 ° both to the horizontal and vertical axis, with the consideration of the earth magnetic field in that particular test field. For the future field application, the field rotation tests should be operated at the particular job site before the installation of the smart rocks, to search the maximum magnetic field intensity angle for the consideration of largest capacity of the installed “smart rock” systems.

Preliminary Results for Waterproof Encasements: To meet the requirements of bridge scour monitoring, both passive and active smart rocks are needed to be packaged in individual waterproof close space with consideration of longer service life. Thus, in this quarter, a waterproof sealant is proposed for this packaging purpose, by joining two hemispheres together and creating a solid sphere. Taking into account of the recycling of the smart rocks for sensing, it is desirable to use a sealant that is not permanent to allow for removal of the smart board once the testing is complete. Thus, in this study, the caulking sealant manufactured by Geocel® Water Shield was selected for the initial testing.

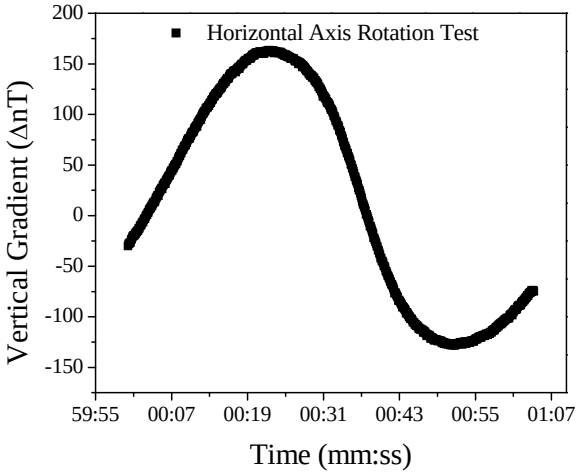

(a) Vertical gradient change for rotation about horizontal axis

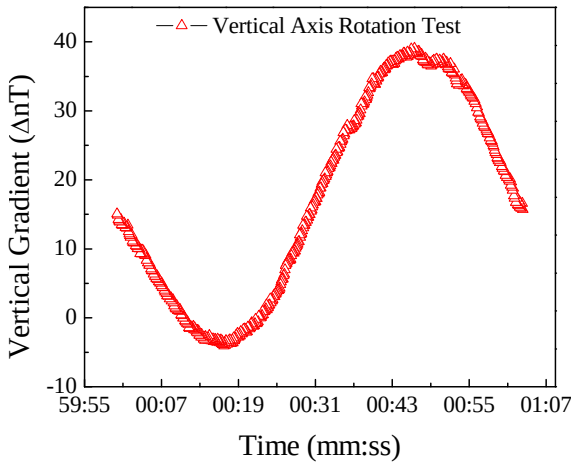

(b) Vertical gradient for rotation about vertical axis

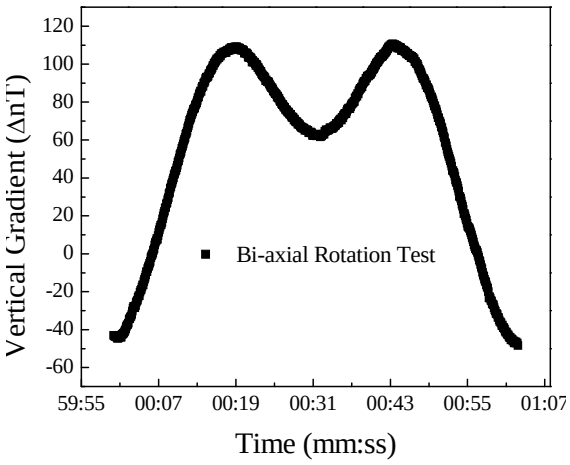

(c) Vertical gradient for a bi-axial rotation

Figure 3: Constant rotation data of a ½" x 1" cylindrical rod magnet

Initial design: A bead of ¼" was placed around the edge of one hemisphere and the second was placed on top. This was held in place to allow the sealant to solidify. The sealant was then tooled to maintain a smooth sphere on the exterior surface. The sealant was allowed to dry for the recommended 24 hours before submerging the sphere in water. The fabricated sphere was submerged into a water tank for one hour to measure the effectiveness of the sealant. After the first hour the sphere was removed and a visual inspection was performed to evaluate whether any water was in the sphere. This process was then repeated for three hours to determine whether an extended period of time submerged would affect the sealant in any adverse manor. After being submerged for three hours there was no leakage of water into the sphere, however, the two halves started to move by the end of the third hour as the sealant began to soften. This should be sufficient in protecting the smart board for any preliminary test necessary as the sphere shouldn't need to be submerged for more than three hours. For long-term testing, alternative sealants are needed.

Task 1.2 Steel Interferences to Magnetic Measurements

Activities in this task will be reported next time.

Task 2.1 Active Smart Rocks with Embedded Controllable Magnets or with Embedded Electronics

"Frictionless" surface: In addition to the packaging of smart rocks, for an active smart rock with a magnet rotated by suddenly powering a coil system wrapped outside the smart rock, a low friction surface to allow for maximum rotation of the magnet within the coil system is also desired. With a design of less friction of the magnet rotation, coil driven fast speed rotation of the magnet could be obtained and therefore whether the fast rotation of the magnet would increase the detection limit of the passive smart rocks can then be determined and testified.

The initial design first included a magnet encased within a hollow sphere with an outside diameter of 1 ½ in. The encased magnet was then placed inside a larger hollow sphere with an outside diameter of 2 in. Finally, a membrane of general motor oil had been applied between the two spheres to reduce the friction in between as displayed in Figure 4. However, this design is prone to a weight imbalance due to the variability of the magnet placement within the inner sphere. In an effort to overcome the weight imbalance, a second version of the frictionless surface is developed as discussed below.

Figure 4: Oil encased magnet

The second version of the packaging sphere design has a few variations from the first design. For a correction of the weight imbalance problem, the new inner sphere is completely solid. A hole will be drilled through the center of the sphere at a depth of 1 ¼ in. This ensures the 1 in. magnet will be centered and balanced within this sphere. The ¼ in. hole will then be filled with a two part acrylic resin of the same specific gravity as the rest of the acrylic sphere. What is more, instead of using general motor oil, a clear silicone fluid with a low viscosity (5 cSt) and surface tension (19.7 dynes / cm) value will act as the "frictionless" membrane between the two spheres. The lower surface tension ensures less energy needed to turn the magnet encased in the inner sphere.

Task 2.2(a) Magneto-Inductive Communications – Engineering Design and Validation of Magneto-Inductive Transponders

Smart Rock 2.4 Circuitry A total of six smart rock 2.4 boards are currently produced and electrically assembled. Both synchronous and asynchronous Binary/ASCII data transmissions are implemented in smart rock embedded software.

Smart Rock Assembly Figure 5 shows the assembly scheme of a smart rock 2.4 module. It includes the PCB with electronic components, battery and antenna modules enclosed in the 2.5" sealed plastic sphere. Figure 6 shows the photo of a prototype operating on the integrated battery. The ferrite core antenna is visible on top of the board within the shell.

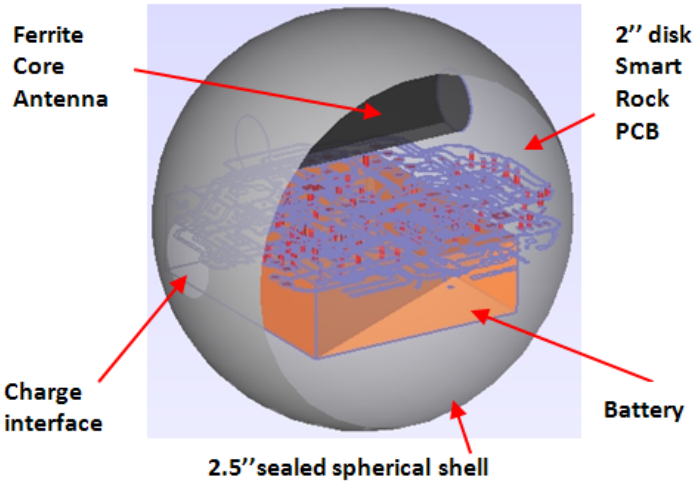

Figure 5: Smart rock 2.4 assembly scheme


Figure 6: Actual product

The antenna is constructed of 125 turns of coil over the ferrite core in one layer (Fair-Rite Products Corp, 3078990911, ui=2300). This provides a 0.57-0.58 mH inductance / 1.2 ohm DC resistance. To tune the antenna at 125 KHz, 0806 package size 25V capacitors of 2.7 nF are used. For the transmitter, the capacitors are connected in series to the antenna providing the maximum current flow (acceptor circuit). For the receiver, they are connected in parallel (rejector circuit), providing the best sensitivity to the external field.
Single CR123A 3V 1550 mAh battery fits the shell sphere assembly well and is capable of providing sufficient current for laboratory tests of smart rock 2.4. Rechargeable RCR123A 1000 mAh units are also available.

Base Station Transmitter Interface By default, a smart rock is in low power consumption sleep mode and can be waked up by timer or by external request signal. A smart rock uses several modules placed close to each other. To avoid data collision and effectively process the data transmitted by the smart rock, it is important that one active module operates at any time. Therefore, a control needs to be provided to the smart rock system operator such that the single smart rock module can be selected, waken up and read out. The data-exchange channel needs to be established between the base station and the selected smart rock module. Figure 7 shows a scheme of the corresponding interface involving Control Board, Power Amplifier and a transmitting antenna.

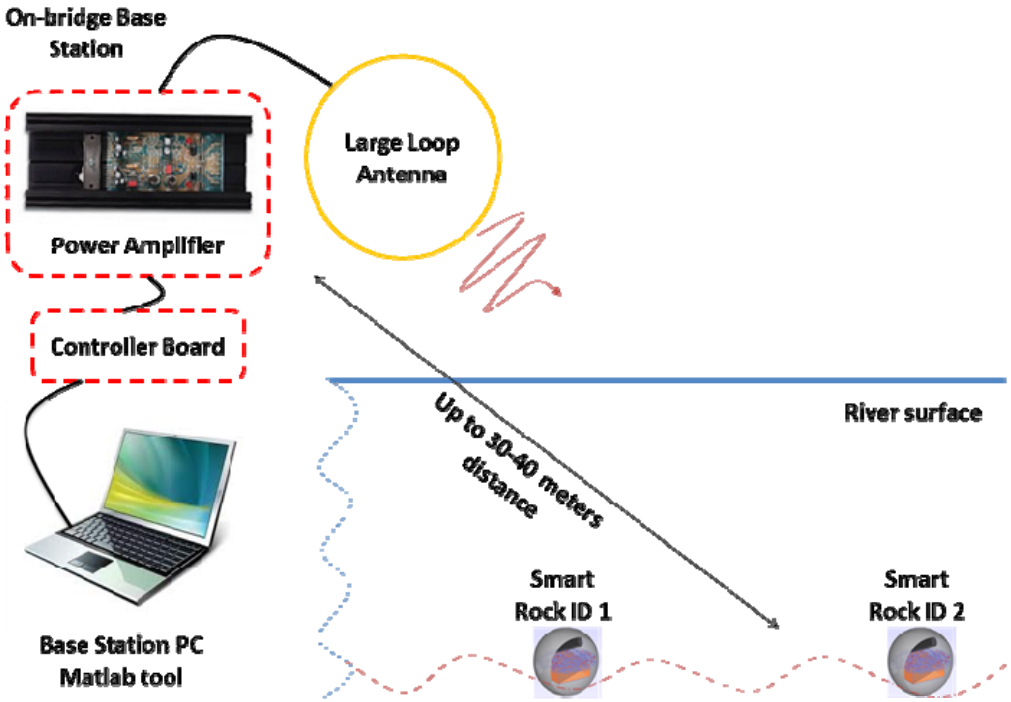

Figure 7: Base station interface for smart rock wake-up signal transmission

At the base station, power consumption is not an issue. As such, high power amplifiers and large scale (high efficient) antennas can be applied to produce necessary field strength of the transmitted wake-up signal at considerably large distances and complex environmental conditions. The software PC control core is implemented in Matlab and currently is under revision and GUI design stage. The Velleman K4004B 200W amplifier kit was ordered and assembled. The base station transmitter design is independent of the smart rock modules used and can be applied for both miniaturized smart rock 2.4 and normal large-scale smart rocks. Developed software is flexible for modifications in case further adjustments are needed.

Based on a theoretical estimation for the smart rock 2.4 ferrite core antennas and the used transmitter amplifier/antenna pair, the achievable wake up distance exceeds 30 m. In practice this distance may be less but definitely sufficient for laboratory tests.

Base Station Transmitter Controller Board The interface controller board was designed based on the same microcontroller as it is used on smart rock 2.4 – PIC16LF1823. It also features MAX232 IC for processing of the data sent from the base station PC through the serial interface (COM port, RS 232). Figure 8 shows a photo of the control board labeling all of the key components. The embedded software translates commands received from the operator PC into the specific wake-up signal pattern required by the smart rock 2.4 on-board receiver module (AS3930) with corresponding ID integration and it does not require to pre-program particular ID signatures (no need to reprogram the board if a new smart rock module becomes available and used for scour monitoring).

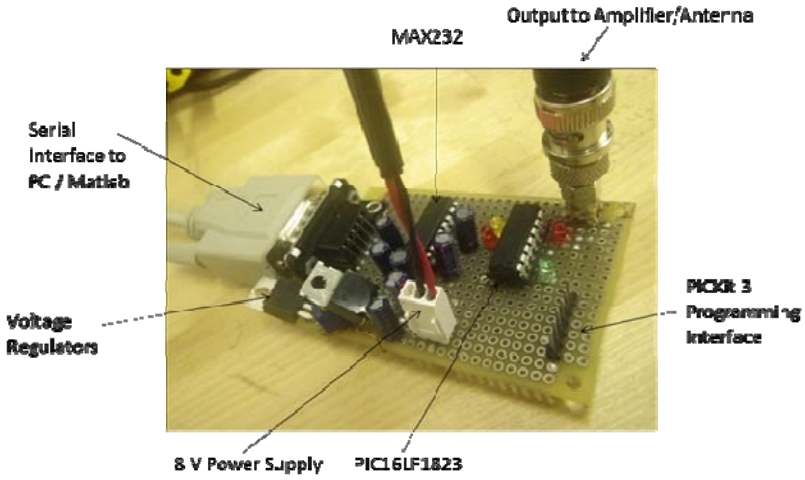

Figure 8: Base station transmitter controller board

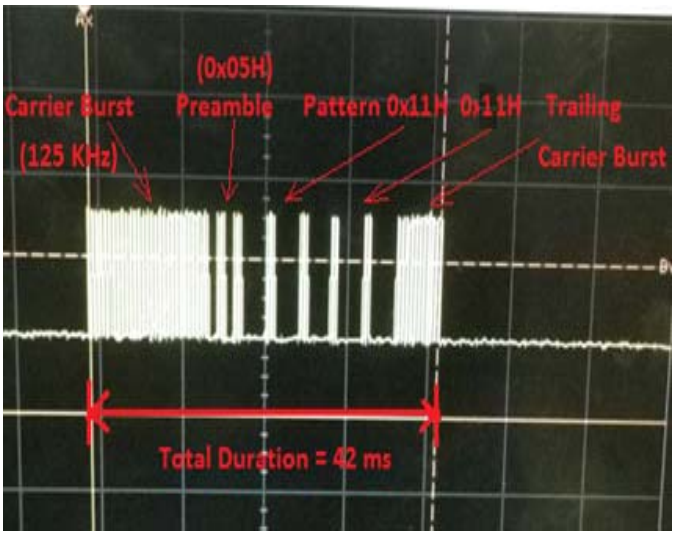

Figure 9: Typical wake-up signal

Figure 9 shows a typical wake-up signal generated by the controller board. It includes a carrier burst followed by the preamble, ID pattern and the trailing. As specified by the minimum specifications of the AS3930, the minimum value of data rate supported is 1024 bits/s or 512 Manchester Symbols/s. Therefore, the data rate for the above signals – preamble and pattern, is set to 1024 bits/s by programming the microcontroller accordingly.

Task 2.2(b) Acoustic Communications – Engineering Evaluation of Acoustic Communication Systems for Bridge Scour Monitoring

In this quarter, our work was focused on improving the robustness of the receiver implementation on the DSP platform. We first refined Matlab simulation of the transmitter and receiver solutions, then redesigned the C++ solutions accordingly and debugged the hardware implementation on the TI DSP platform.

For the Matlab simulation part, we designed PN sequence to replace the previous 7-bit Barber code as the preamble ID for “Start of the Frame”. The PN code now is a 15-bit m sequence with a generator polynomial gen = [1 0 0 1, 0 0 1] and a seed seed= [1 0 0 1, 0 1 0 1, 0 0 0 0, 0 0 0 1]; The resulting PN code is ID_code = [0 1 1 1, 1 0 0 1, 1 0 1 1, 0 0 0]. The transmission data rate is 5 kpbs now and can be modified as needed easily. The data bits are represented by rectangular pulse shaping and on-off keying modulation with 125 kHz carrier frequency.

The receiver uses 55 kHz band-pass sampling followed by a band-pass filter of 69 taps, a full rectifier, and then matched filters. Signal energy detector and PN code correlator are also implemented with dynamic threshold setting and correlation peak detection. The receiver input and output signals are shown in Figure 10. The processed receiver signals are shown in Figure 11. Here, Figure 11 (a) shows the rectified received signal and MF output aligned by adding corresponding group delays. Figure 11 (b) shows the correlator output where the peak is identified perfectly at the end of the ID code.

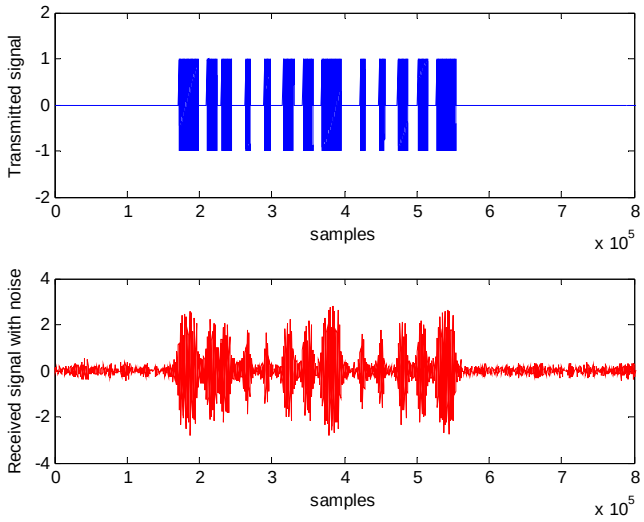

Figure 10: Tx and Rx signals

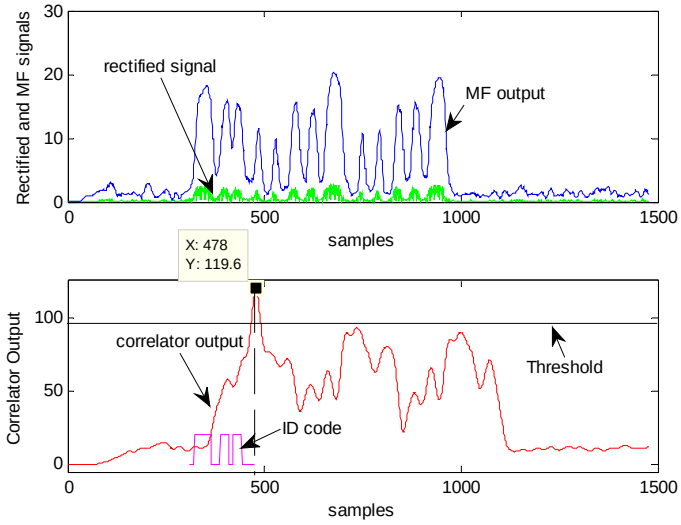

Figure 11: Rx signals and MF & Correlator outputs

The peak detection algorithm is shown below:

```
% digital differentiator to detect the peak in Rx_corr
for k= group_delay: length(Rx_corr)
   if (Rx_corr(k)>Th) && (foundpeak == 0)
      dc_k= abs(Rx_corr(k-1))-abs(Rx_corr(k+1)) + 2*(abs(Rx_corr(k-2))-
abs(Rx_corr(k+2)));
      dc_k1= abs(Rx_corr(k))-abs(Rx_corr(k+2)) + 2*(abs(Rx_corr(k-1))-
abs(Rx_corr(k+3)));
      if (dc_k <0) && (dc_k1 >= 0)
         if abs(Rx_corr(k+1)) >abs(Rx_corr(k))
            index_k= k+1; %index of peak = start of data block
         else
            index_k=k; %index of peak = start of data block
         end
         foundpeak =1;
      end
   end
end
```

Note that the correlator output is twice as long as the ID code. Therefore, the peak search has to be performed for two times the length of ID code. Once the ID code is detected, the peak index identifies the start of the frame with the accuracy of Ts/2, where Ts= sampling rate/ symbol rate. This accuracy can be improved by increasing the symbol rate to 10 kbps. That is the required timing accuracy for time-difference of arrival detection.

The symbol detection is followed after the correlator peak is identified. Another threshold is applied to the MF output. The signal above threshold is detected as bit 1, otherwise bit 0.

For the TI DSP hardware implementation, the receiver detection has been redesigned according to the new Matlab algorithm. Filter coefficients are converted to integer types and signal thresholds are recalculated accordingly. Filter implementation has been refined to get rid of multi-layers of nested “for” loops so that the processing is more efficient. Several bugs were also identified and fixed with the EDMA control program. The problem with lost data bits has been fixed with the new EDMA control logic and the improved receiver processing. The CCS v4 outputs are shown in Figures 12-14, where Figure 12 shows 2000 samples of rectifier output of the received signal after band-pass filtering. Note the results match the Matlab simulation results in Figure 11 (a). Figure 13 shows 4000 samples of match filter output that has been implemented by moving sum. The matched filter also serves as low-pass filter to remove the carrier frequency. This also matches the Matlab results shown in Figure 11. Figure 14 shows the signal power estimator output that will be used to set dynamic threshold for ID code correlator. Note that the signal energy matches the MF filter output patterns. The correlator is currently being coded and implemented in C++. The bit detection has been implemented successfully. The over test of the hardware implementation is still required.

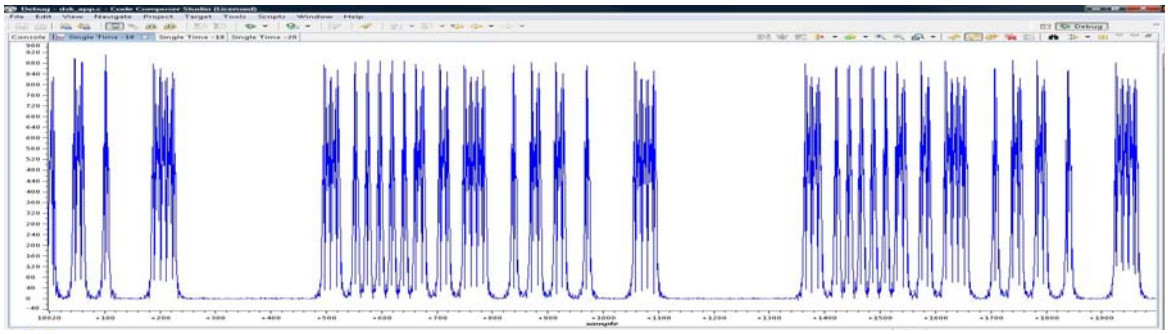

Figure 12: Received signal after rectifier recorded by DSP CCS results

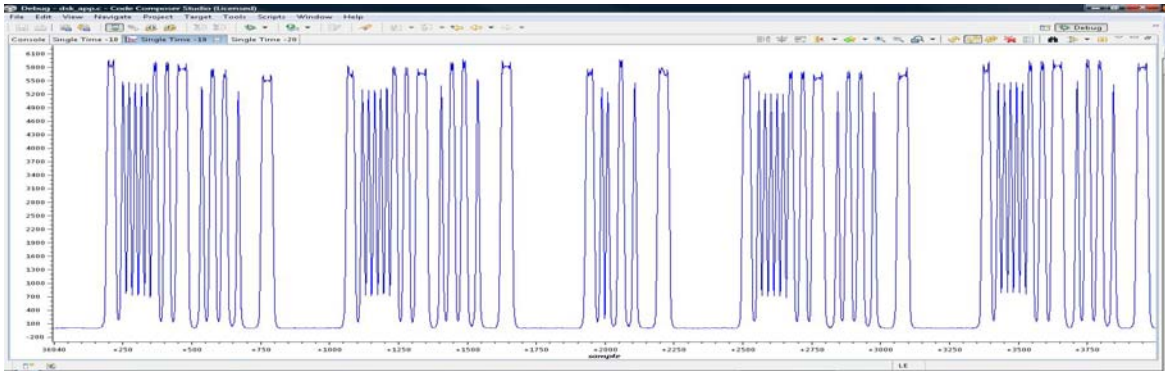

Figure 13: Matched filter output recorded by DSP CCS results

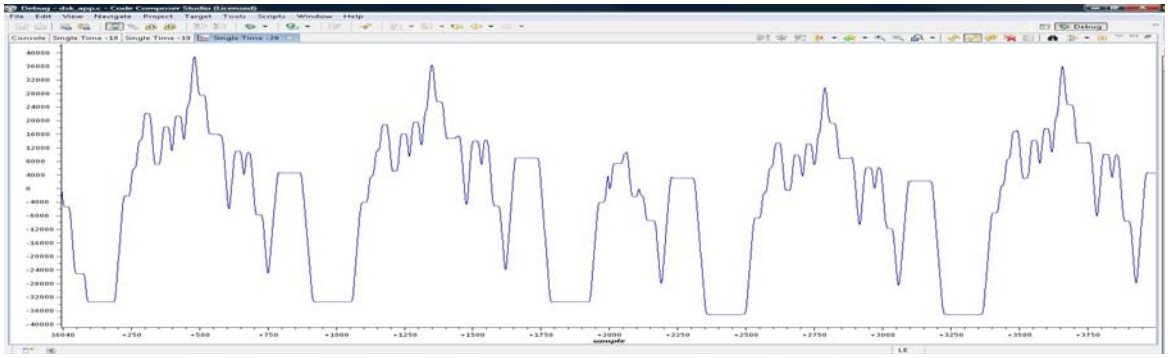

Figure 14: Symbol energy detector output for dynamic threshold setting

Task 3.2 Field Validation Planning and Execution

Field test plan just begins in April. It is expected that some field tests are done by June 30 and results are reported in the next report.

I.2 PROBLEMS ENCOUNTERED

During the third quarter of the project, no unexpected technical problem was encountered. The overall technical work is slightly delayed due to unfilled post doctor position.

A new post-doctoral fellow has been recently identified and will part-time participate in this project starting in April. One Ph.D. and one M.S. students are currently supported on this project.

I.3 FUTURE PLANS

Three subtasks will be executed during the next quarter. A brief description of various activities in each subtask is described below:

Task 1.1 Design, fabricate, and test in laboratory and field conditions DC magnetic sensors with embedded steel in Dodecahedron shape or magnets aligned with the earth gravity field. Summarize and document the test results and the performance of passive smart sensors.

Built on the previous work, laboratory tests on passive smart rocks with embedded permanent magnets will start in the following performance period. Their effectiveness in providing sensitive magnetic field measurements will be systematically characterized.

Task 1.2 Research, summarize, and document the degree of potential steel interferences to magnetic measurements. Investigate ways to compensate the interference effect and develop a rock localization technique.

Laboratory work will begin to test potential interference of ferrous objects on magnetic field measurements.

Task 2.1 Design, fabricate, and test in laboratory and field conditions active smart rocks with embedded controllable magnets or with embedded electronics. Summarize and document the test results and the performance of active smart rocks.

The design of active smart rocks with controllable magnets is currently under way. The test results will be reported during the following quarterly report.

Task 2.2(a) Design, fabricate, and test in laboratory and field conditions magneto-inductive transponders. Summarize and document the test results and the performance of transponders.

The smart rock 2.4 products are ready for further system integration with Digital Signal Processing modules. The next generation of smart rocks will be integrated with on-board memory modules to perform a date/time stamped log of significant movements of the smart rock based on accelerometer tilt/roll interrupts. Laboratory tests for position change effects will be reported in the next report.

Task 2.2(b) Research, summarize, and document current underwater acoustic transmission practices and required modifications for bridge scour monitoring.

In the following quarter, the acoustic communication system with transmitter and receiver will be refined. A multi-receiver system will then be built and tested with capability of smart rock localization. In this case, multiple transducers / hydrophones are distributed to different locations for TDOA estimation. The smart rocks will be located using the TDOA fusion and the assistance of pressure sensor in smart rocks, which provides the elevation information of the smart rocks. They will be ready for field testing of one or two bridges.

Task 3.2 Plan and execute the field validation tasks of various prototypes. Analyze the field performance of smart rocks and communication systems.

As prototype smart rocks are being designed and built, field test plan will be developed during the following report.

II – BUSINESS STATUS

II.1 HOURS/EFFORT EXPENDED

The planned hours and the actual hours spent on this project are given and compared in Table 1. In the third quarter, the actual hours are approximately 50% of the planned hours due to short of staff appointed on this particular project. That is, the actual cumulative hours are approximately 40% of the planned hours. The cumulative hours spent on various tasks by personnel are presented in Figure 15.

Table 1 Hours Spent on This Project

	Planned		Actual	
	Labor Hours	Cumulative	Labor Hours	Cumulative
Quarter 1	752	752	184	184
Quarter 2	752	1504	345	529
Quarter 3	752	2256	381	909

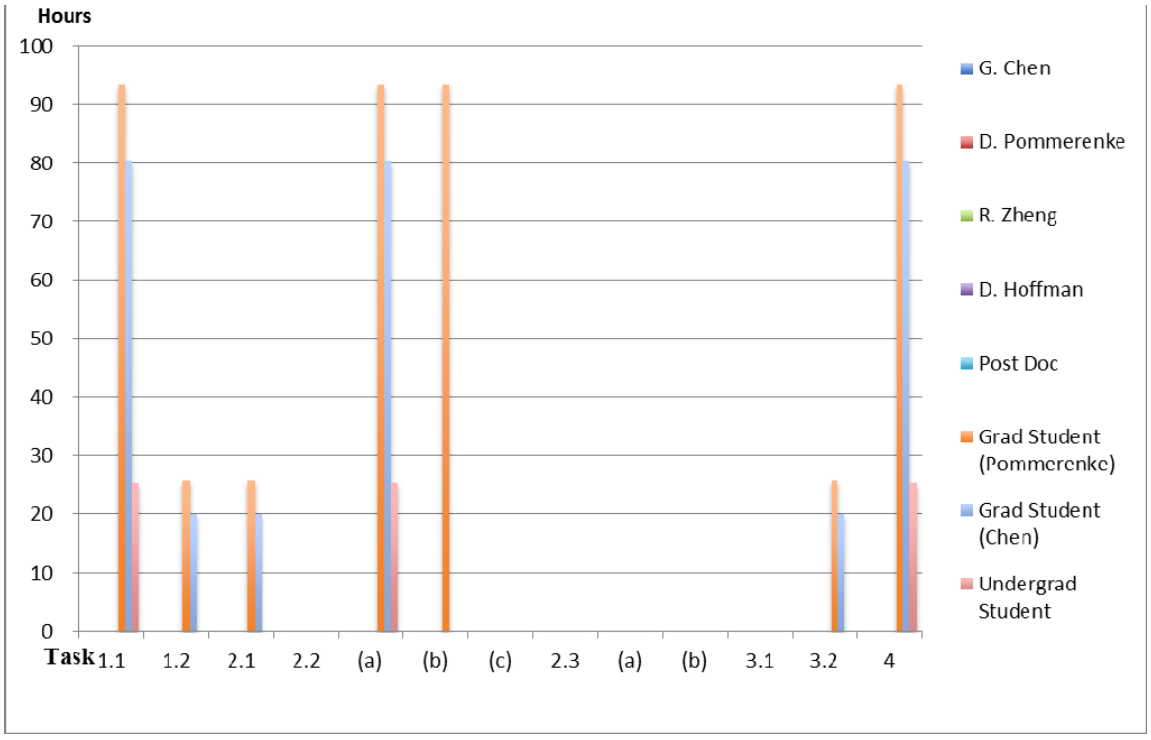

Figure 15 Cummulative hours spent on various tasks by personnel

II.2 FUNDS EXPENDED AND COST SHARE

The budgeted and expended RITA funds in each quarter are compared in Figure 16. Approximately 42% of the budget has been spent during the third quarter. The actual cumulative expenditures from RITA and Missouri S&T are compared in Figure 17. It can be seen from Figure 17 that the expenditure from RITA is approximately 82% of that from the Missouri S&T. Their ratio (RITA to Missouri S&T) is less than 1.0, which meets the minimum match fund requirement.

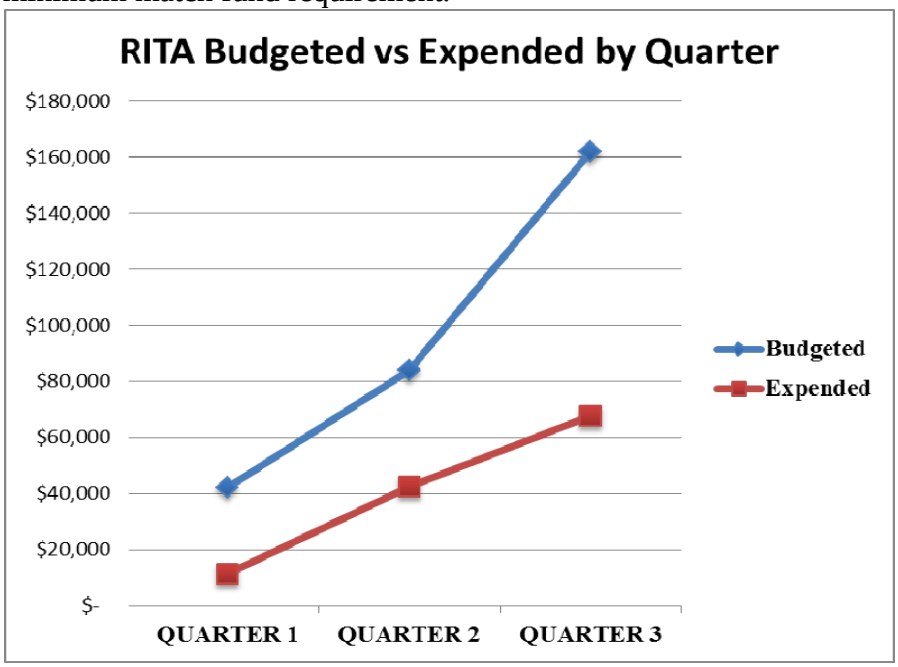

Figure 16 RITA budget and expenditure comparison in every quarter

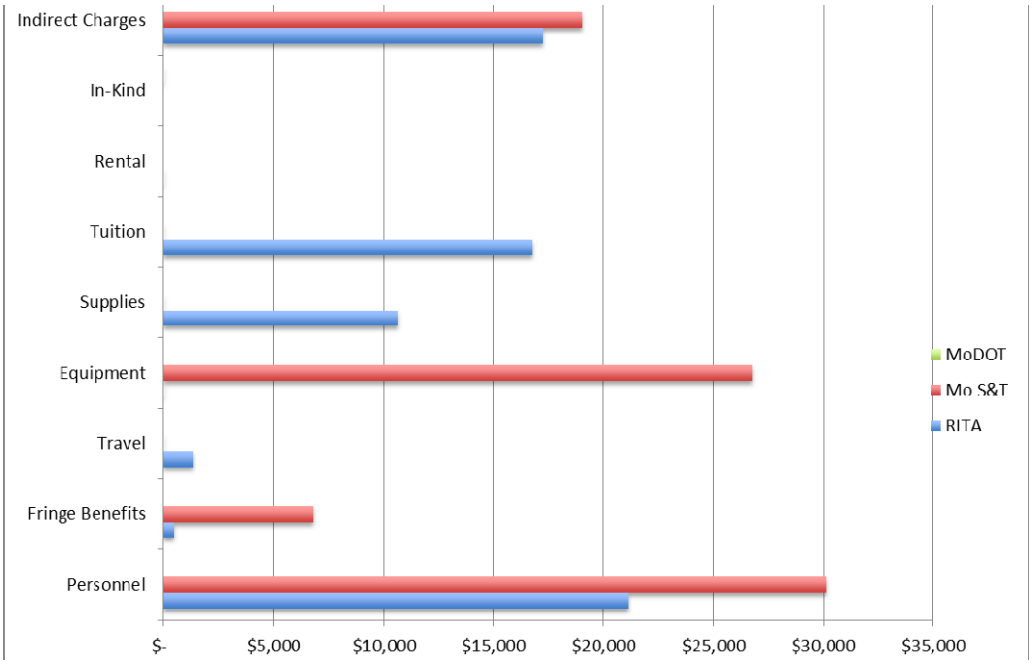

Figure 17 Cummulative expenditures by sponsor